ADVANCES IN ATMOSPHERIC SCIENCES, VOL. 24, NO. 2, 2007, 281–300

Impact of 4DVAR Assimilation of Rainfall Data on the Simulation of Mesoscale Precipitation Systems in a Mei-yu Heavy Rainfall Event

CHU Kekuan[1] (储可宽), TAN Zhemin*[1] (谈哲敏), and Ming XUE[2]

[1]*Key Lab of Mesoscale Severe Weather/MOE and Department of Atmospheric Sciences, Nanjing University, Nanjing* 210093

[2]*School of Meteorology and Center for Analysis and Prediction of Storms, University of Oklahoma, Norman, OK* 73019*, USA*

(Received 16 March 2006; revised 6 July 2006)

ABSTRACT

The multi-scale weather systems associated with a mei-yu front and the corresponding heavy precipitation during a particular heavy rainfall event that occurred on 4–5 July 2003 in east China were successfully simulated through rainfall assimilation using the PSU/NCAR non-hydrostatic, mesoscale, numerical model (MM5) and its four-dimensional, variational, data assimilation (4DVAR) system. For this case, the improvement of the process via the 4DVAR rainfall assimilation into the simulation of mesoscale precipitation systems is investigated. With the rainfall assimilation, the convection is triggered at the right location and time, and the evolution and spatial distribution of the mesoscale convective systems (MCSs) are also more correctly simulated. Through the interactions between MCSs and the weather systems at different scales, including the low-level jet and mei-yu front, the simulation of the entire mei-yu weather system is significantly improved, both during the data assimilation window and the subsequent 12-h period. The results suggest that the rainfall assimilation first provides positive impact at the convective scale and the influences are then propagated upscale to the meso- and sub-synoptic scales.

Through a set of sensitive experiments designed to evaluate the impact of different initial variables on the simulation of mei-yu heavy rainfall, it was found that the moisture field and meridional wind had the strongest effect during the convection initialization stage, however, after the convection was fully triggered, all of the variables at the initial condition seemed to have comparable importance.

Key words: 4DVAR, rainfall assimilation impact, mesoscale convective system, mei-yu heavy rainfall

DOI: 10.1007/s00376-007-0281-9

1. Introduction

The mei-yu (or Changma in Korea and Baiu in Japan) front is the most important weather system in East Asia and dominates the warm weather rainfalls in East Asia, especially in the downstream region of the Yangtze River (hereafter referred to as DRYR) in China. The mei-yu system contains weather ranging from the meso- to synoptic scales. In general, the mei-yu front is a moist, quasi-stationary front with weak baroclinicity; it has a weak meridional gradient in temperature but a strong moisture gradient. Usually, many mesoscale convective systems (MCSs) exist in the mei-yu front that are at different stages of their life cycles and are triggered mainly by the localized features (Chen et al., 1998, 2000). These MCSs are the main causes of the continual heavy rainfall and flooding in DRYR during the warm seasons. Moreover, there exist other weather systems, such as the low level jet that contribute to the mesoscale precipitation systems within mei-yu front (Chen et al., 2005). From a forecast perspective, accurate quantitative precipitation forecasts (QPF) of mei-yu heavy rainfall events remain a difficult task. The correct forecasting of when and where the MCSs are triggered and of their subsequent evolution is also critical in improving the QPF

*E-mail: zmtan@nju.edu.cn

associated with other mei-yu systems. The current networks of conventional observations are unable to provide sufficient information for accurately initializing the Numerical Weather Prediction (NWP) model with sufficient high resolution. Furthermore, the understanding of the physical and dynamical mechanisms of the genesis, evolution and maintenance of the convective precipitation systems within the mei-yu systems is far from complete. Therefore, research efforts aimed at trying to improve the estimates for the initial conditions, thereby allowing reductions in the uncertainties, of the forecasting of the mei-yu weather systems are challenging, yet very valuable. One way to improve these estimates is through the assimilation of rainfall data that are often available from dense surface rain gauge networks. Although the uncertainty in the lateral boundary conditions, as well as the model uncertainties, can also be significant, we neglect them here in order to isolate the uncertainties in the initial conditions.

Rainfall observations were first incorporated into numerical weather prediction (NWP) models in the literature through initialization processes. Many initialization schemes, such as the dynamical initialization (Fiorino and Warner, 1981), physical initialization (Krishnamurti et al., 1991, 1993) and cumulus initialization (Donner, 1988) have been developed and notable positive impacts have been reported. In the initialization processes, the rainfall observations are mainly used to modify the thermodynamic properties, such as the temperature and moisture fields, so as to remedy the precipitation spin-up problem and to improve the short-range quantitative precipitation forecasts. All these studies have shown the effectiveness of these initialization schemes. However, initialization is an indirect way of using precipitation data, after all, it cannot guarantee the dynamical consistency among all of the initial fields. Directly using rainfall observations via four-dimensional variational data assimilation (4DVAR) is more desirable, as it can adjust all of the initial fields in a dynamically and physically consistent way.

This study focuses on the use of the 4DVAR method and its advantages over other assimilation approaches that have been discussed, (e.g., Zou and Kuo, 1996; Park and Zupanski, 2003). The 4DVAR assimilation of the precipitation data was first shown to outperform the conventional data assimilation method of optimal interpolation (OI) in precipitation forecast by Zupanski and Mesinger (1995). Zou and Kuo (1996) demonstrated the ability of the 4DVAR assimilation of the precipitation in capturing the detailed structure of the mesoscale features in the initial conditions, which was crucial for the forecast of the MCSs in their case and for reducing the spin-up time required for precipitation development. Other works, such as Guo et al. (2000) and Zupanski and Zupanski (2002) also showed the improved performance of the 4DVAR assimilation in the study of a strong convective and a winter snow storm case, respectively. In addition to conventional rainfall data, the 4DVAR assimilation of other kinds of precipitation data can also be very useful. Data that have been examined include the SSM/I precipitation rate data from remote sensing satellites for tropic cyclone simulations (Tsuyuki, 1997), the NCEP multi-sensor hourly rainfall data for the simulation of a squall line case (Peng and Zou, 2002) and TRMM Microwave Imager (TMI) derived rainfall data on the simulation of Hurricane Bonnie (1998) (Pu and Tao, 2004).

Although significant progress has been achieved through 4DVAR assimilation of several types of precipitation data, the ability of a 4DVAR scheme in assimilating short-range precipitation of a large amounts and the impact of such assimilation on the heavy rainfall events associated with mei-yu fronts have not been sufficiently studied thus far. Wang et al. (2004) discussed the influence of the different assimilation variables and weighting coefficients on the assimilation of precipitation in a real mei-yu frontal rainstorm case and showed the 4DVAR assimilation to have a potential in mei-yu frontal rainfall forecasting. In this paper, based on assessing the ability of a 4DVAR assimilation of rainfall data for a mei-yu heavy rainfall case, we focus on the understanding of how the assimilation impacts the precipitation and the mesoscale precipitation systems simulation in dynamics.

The rest of this paper is organized as follows. Section 2 presents a brief synoptic overview of the case. The numerical model, datasets, the data assimilation system as well as the experimental design are described in section 3. Section 4 discusses the results in detail. In section 5, a discussion of an additional set of sensitive experiments that were conducted to assess the impact of the analysis increment of each initial field on the heavy rainfall simulation is provided. Finally, conclusions and discussions are given in section 6.

2. Synoptic overview

During the 2003 mei-yu season, a particularly heavy rainfall event occurred on July 4–5 in the DRYR, especially in the Henan, Anhui and Jiangsu Provinces. The heavy rainfall was mainly a result of a successive sequence of MCSs embedded in the mei-yu frontal system. These MCSs developed and became mature between 1200 UTC 4 July and 0000 UTC 5 July 2003, thereby producing a maximum 12-h obser-

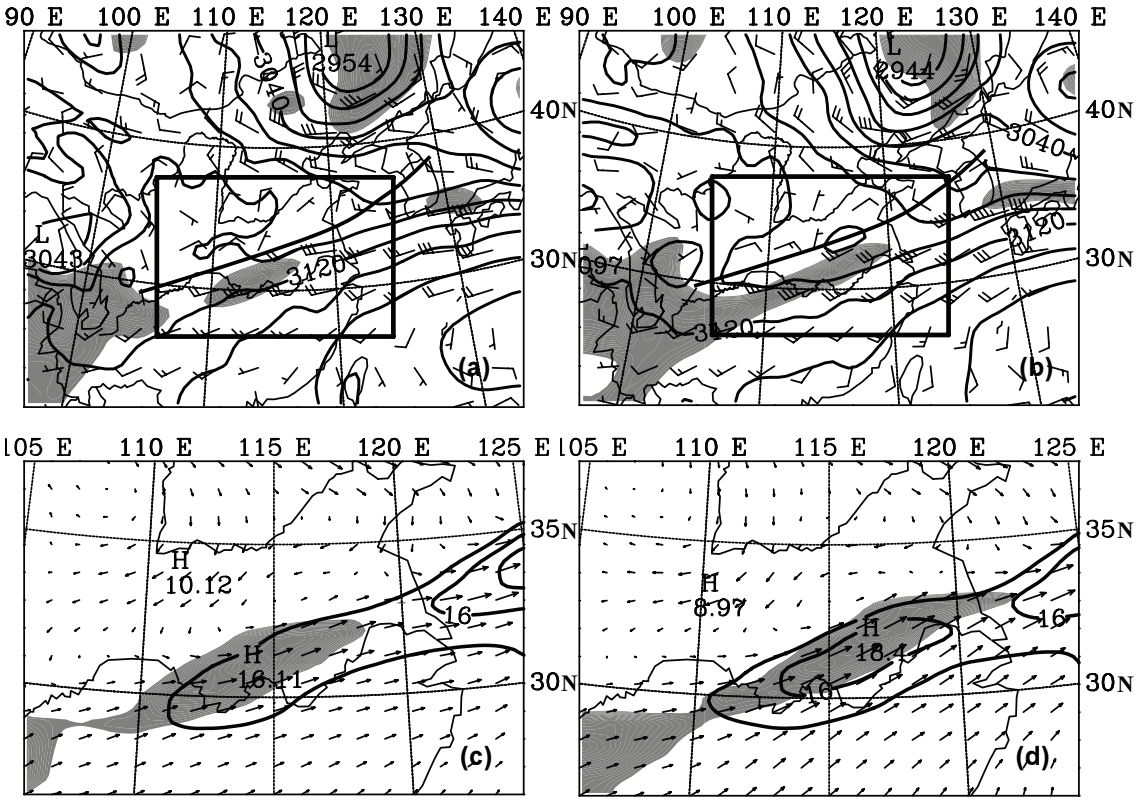

Fig. 1. Upper panel: The NCEP global analysis geopotential height (solid contours), relative humidity (shaded, with relative humidity greater than 80%) and horizontal wind barbs at 700 hPa at (a) 1200 and (b) 1800 UTC 4 July 2003. Lower panel: The horizontal wind speed (solid contours $\geqslant$12 m s^{-1} at 2 m s^{-1} intervals), specified humidity (dashed contours $\geqslant$ 10 g kg^{-1}), and wind vectors at the same level, at (c) 1200 and (d) 1800 UTC, plotted for a 20 km grid-spacing sub-domain indicated by the rectangular box in the upper panel. Wind barbs and vectors are plotted every 3rd grid point. The bold, south-southwest to north-northeast oriented line in the upper panels indicates a line with strong directional shear and wind convergence, commonly referred to as a shear line.

ved rainfall of about 240 mm.

Figure 1 shows the 700 hPa geopotential height, relative humidity and horizontal wind fields at 700 hPa in the upper panel and in the lower panel the horizontal wind speed, specific humidity and wind vector fields in a subdomain for 1200 and 1800 UTC 4 July 2003 are presented. These fields are interpolated from the NCEP $1^\circ \times 1^\circ$ operational analyses to the 60 and 20 km plotting domains, respectively. At 1200 UTC 4 July 2003, before the onset of most of the MCSs, a weak trough associated with a strong shear line existed over the DRYR (Fig. 1a) and extended to the southwest. A low-level jet (LLJ), with horizontal wind speeds greater than 12 m s^{-1}, existed to the immediate south of the shear line and extended northeastward of Hubei Province, and was accompanied by a moisture tongue that extended in the same direction (Fig. 1c). The low-level jet supplied the mei-yu front at the lower reaches of the Yangtze River with rich, warm and moist air from the Indian Ocean and the South China Sea. Six hours later, the weak trough deepened somewhat and a small depression with a closed 3130 m gpm height contour formed over Anhui along the shear line that remained at the same location (Fig. 1b). At the same time, the LLJ was also enhanced, with a jet core forming over Hubei and Anhui whose horizontal wind speed exceeded 16 m s^{-1} (Fig. 1b). In addition, the moisture tongue extended much further to the northeast.

The satellite brightness temperature from the GEOS-9 channel one shows (Fig. 2) that at 1200 UTC 4 July, there were several separate convective systems in a line along the Yangtze River within Anhui and Jiangsu provinces; these convective centers were the remnants of an earlier heavy rainfall process and they mostly dissipated within the next two hours. By 1400 UTC, the new convection had started to develop at the tri-province border regions of Henan, Hubei and Anhui. Two hours later, at 1600 UTC, two more regions of convection developed further downstream, along

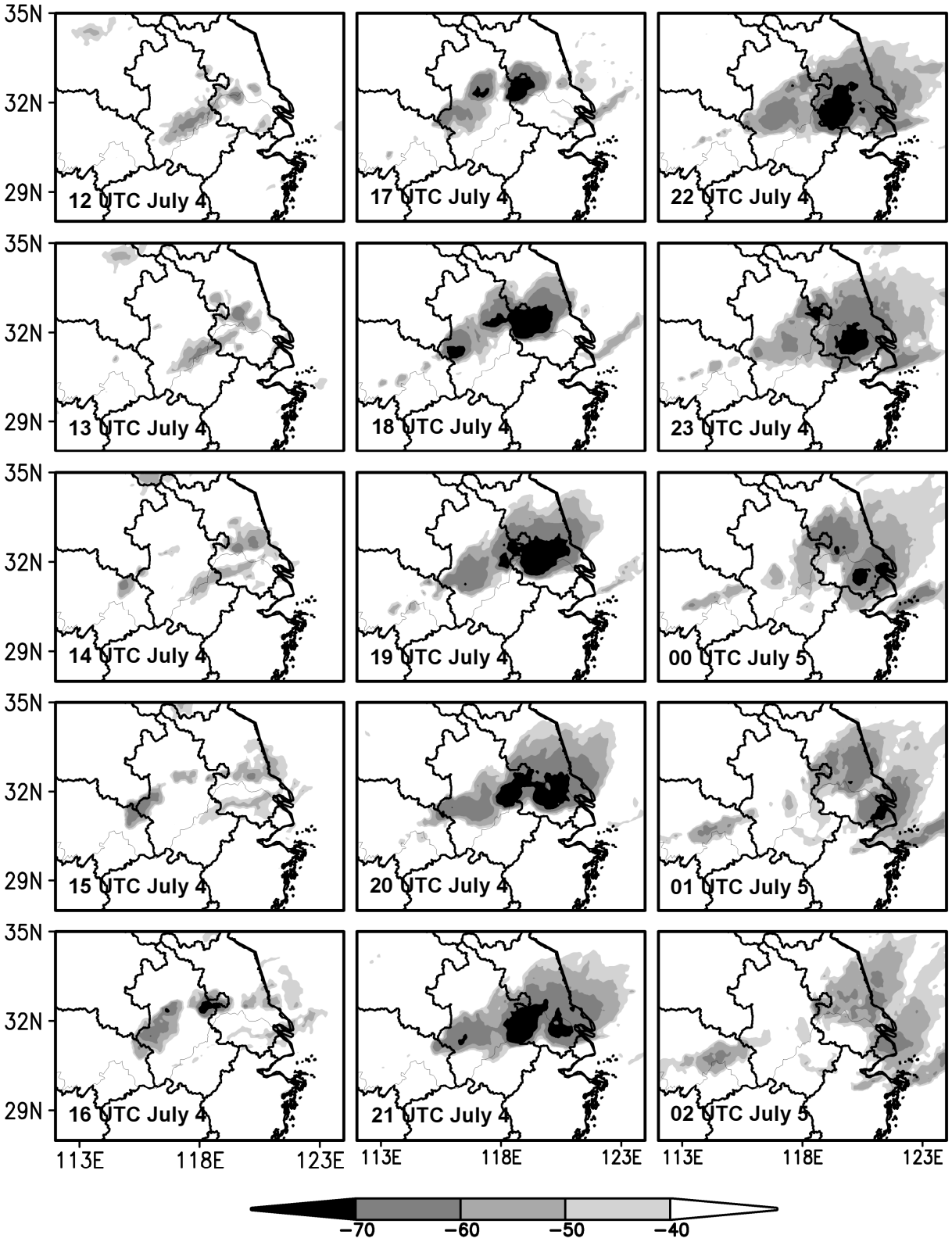

Fig. 2. The satellite brightness temperature (TBB) that was valid between 1200 UTC 4 July and 0200 UTC 5 July 2003, at one hour intervals.

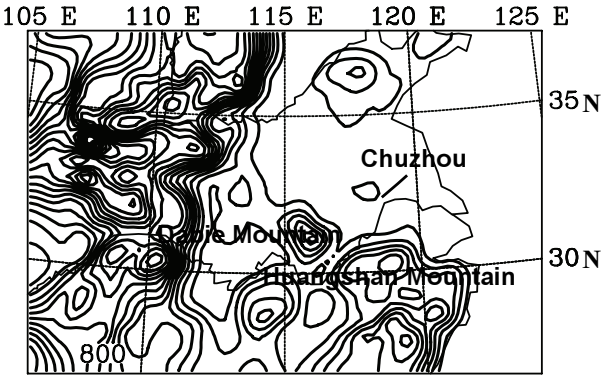

Fig. 3. The terrain contours in the inner domain. Chuzhou is where the soundings will be extracted and plotted later.

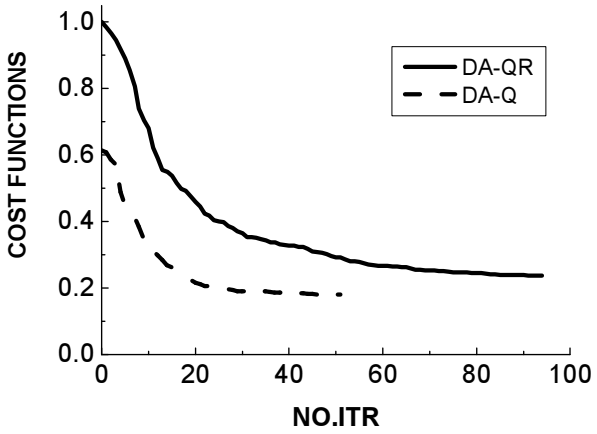

Fig. 4. The variations in the cost functions with respect to the iterations, the abscissa represents the number of iterations and the y-axis represents the normalized cost functions' value. The solid line represents the total cost function in DA-QR and the dashed line represents the cost function in DA-Q.

the river in central Anhui and at the Anhui-Jiangsu border. By 1700 UTC, one can see three separate centers of well developed convection, reaching MCS sizes. These convective centers expand in size over the subsequent hours with the two downstream merging together by 1800 UTC, but with the western most one remaining more or less separate until its eventual decay by about 2300 UTC. These MCSs moved slowly east and remained intense for over 6 hours (Fig. 2). The overall system decay started after 2300 UTC, where they were observed to break up and move out to sea rapidly. Further details on the description of the MCSs during this heavy rainfall event and the influence of different scale weather systems can be found in Liao and Tan (2005).

3. Numerical models and experiments design

The PSU/NCAR limited-area, non-hydrostatic primitive equation numerical model MM5 (Dudhia, 1993; Grell et al., 1995) and its adjoint system (Zou et al., 1997, 1998) are employed in this study for numerical simulation and data assimilation. The vertical coordinates of the MM5 are terrain-following, with $\sigma = (p - p_{\rm top})/(p_{\rm sfc} - p_{\rm top})$, where p is a reference pressure, $p_{\rm top}$ is the pressure at the model top (set to 100 hPa in this study), and $p_{\rm sfc}$ is the surface pressure. The Grell cumulus parameterization, a simple ice microphysics scheme, a simple radiation scheme (Dudhia, 1993) and the Blackadar high-resolution, planetary boundary layer (PBL) parameterization scheme (Blackadar, 1976, 1979; Zhang and Anthes, 1982) are used in this study. Correspondingly, the adjoint of Grell cumulus parameterization, the simple ice microphysics scheme and the high resolution PBL scheme are also used for consistency between the forward and adjoint models.

In general, a 4DVAR system tries to minimize the cost function, which measures the distance between the model solution and the observations over a period called the assimilation window, providing a constraint on the analysis at the initial time of the data assimilation window by the analysis background. With the help of the gradient of the cost function with respect to the model state at the beginning of assimilation window, through backward integration of the adjoint, the cost function is minimized. An optimal estimate of the state of the atmosphere is then obtained that best fits the properly weighted observations and the background.

In this study, the cost function is defined as follows:

$$\begin{aligned} J(X_0) =& \frac{1}{2}(\boldsymbol{X}_0 - \boldsymbol{X}_{\rm b})^{\rm T}\boldsymbol{W}_{\rm b}(\boldsymbol{X}_0 - \boldsymbol{X}_{\rm b}) + \\ & \frac{1}{2}\sum_{i=0,6}\{[U(t_i) - U_{\rm obs}(t_i)]^{\rm T}\boldsymbol{W}_U[U(t_i) - \\ & U_{\rm obs}(t_i)] + [V(t_i) - V_{\rm obs}(t_i)]^{\rm T}\boldsymbol{W}_V[V(t_i) - \\ & V_{\rm obs}(t_i)] + [T(t_i) - T_{\rm obs}(t_i)]^{\rm T}\boldsymbol{W}_T[T(t_i) - \\ & T_{\rm obs}(t_i)] + [Q(t_i) - Q_{\rm obs}(t_i)]^{\rm T}\boldsymbol{W}_Q[Q(t_i) - \\ & Q_{\rm obs}(t_i)]\} + \frac{1}{2}[R(t_6) - R_{\rm obs}(t_6)]^{\rm T}\boldsymbol{W}_R[R(t_6) \\ & - R_{\rm obs}(t_6)] \end{aligned} \tag{1}$$

The first term on the right hand of Eq. (1) represents the background term measuring the distance between the state vector $\boldsymbol{X}_0$ at the initial time and the analysis background field $\boldsymbol{X}_{\rm b}$ that is valid at the same time. Here, vector $\boldsymbol{X}$ includes three wind com-

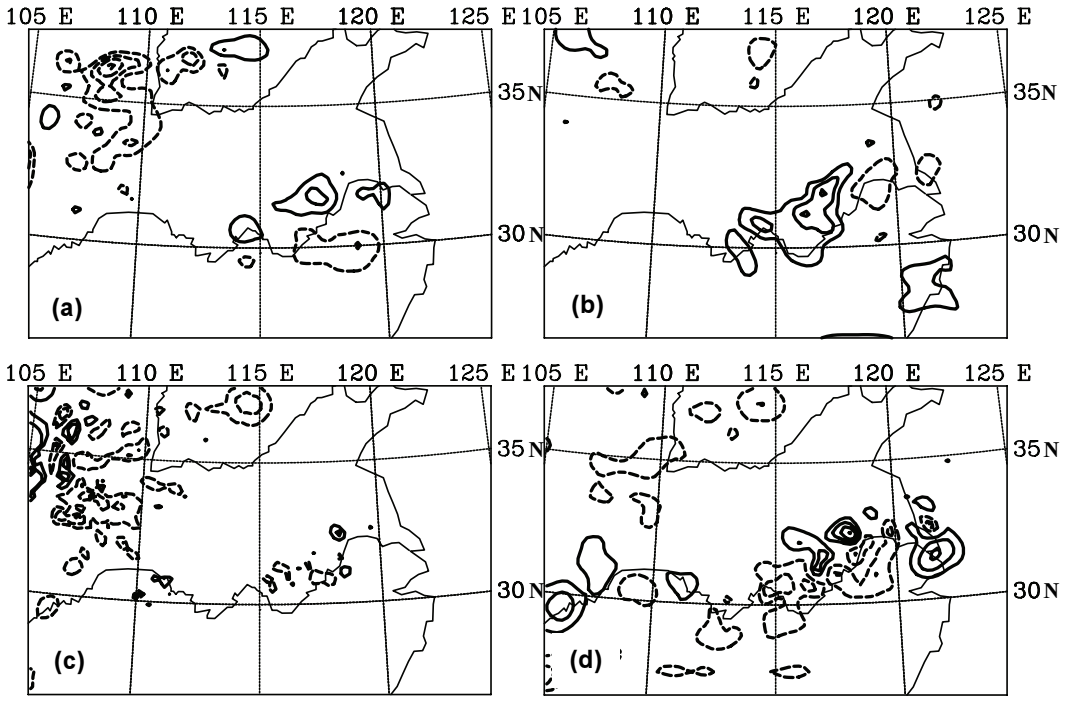

Fig. 5. The differences between the fields at the beginning of assimilation window (1200 UTC 4 July), in DA-QR and CNTL at 850 hPa, for (a) the zonal wind component, (b) medicinal wind component, (c) temperature, and (d) the specific humidity. Negative contours are dashed, and the contour intervals are 1 m s^{-1}, 1.5 m s^{-1}, 0.8°C and 0.5 g kg^{-1}, respectively. Zero contours are not shown.

ponents U, V and $\boldsymbol{W}$, the temperature T, the specific humidity Q, and the perturbation pressure p'. The NCEP $1^\circ \times 1^\circ$ analysis was interpolated into the model grid via the MM5 preprocess procedure that is used as the background or first guess $\boldsymbol{X}_\mathrm{b}$. All other terms on the right hand side of Eq. (1) are the observation constraints for the model variables U, V, T, and Q, and for the 6-hour accumulated rainfall, $R(t_6)$. The observation parts for U, V, T, and Q come from the MM5 analysis combined with the conventional soundings and the NCEP $1^\circ \times 1^\circ$ analysis. $R_\mathrm{obs}(t_6)$ represents the 6-h rainfall observations objectively interpolated into the model grid points using the Cressman scheme. $\boldsymbol{W}_\mathrm{b}, \boldsymbol{W}_U, \boldsymbol{W}_V, \boldsymbol{W}_T, \boldsymbol{W}_Q$, and $\boldsymbol{W}_R$ are diagonal weighting matrices for the background term and for the observation terms corresponding to the observations of the individual quantities. In general, these matrices should be the inverse of the corresponding error covariance matrices. For these observations, when their errors are assumed to be uncorrelated, their matrices are diagonal. For the background term, the covariance matrix is diagonal when the background errors are assumed to be uncorrelated between the variables and in space. The weight matrices are calculated as the inverse of the squared maximum difference between the two analyzed fields that are 6 hours apart (Zou and Kuo, 1996). The rainfall weighting $\boldsymbol{W}_\mathrm{R}$ is set to 4.0 cm^{-2}, corresponding to an empirical 6-hour precipitation measurement error variance of 0.25 cm^2. Considering the large amounts of the observed rainfall, this error variance appears reasonable.

The numerical simulation experiments employed two, two-way nested grids, as shown in Fig. 1. The outer domain (D01) had 49×65 horizontal grid points with a 60-km grid interval. The inner domain (D02) had 61×91 horizontal grid points with a 20-km grid spacing and both domains had a total of 21 vertical layers. The topography within D02 is presented in Fig. 3.

Domain D01 is initialized at 0600 UTC July 4 and D02 domain was started 6 hours later at 1200 UTC July 4. The data assimilation was conducted directly in D02, and the assimilation period or assimilation window length was 6 h, from 1200 UTC to 1800 UTC July 4. We refer to 1200 UTC as the initial time (time zero). The initial conditions at 0600 UTC and the lateral boundary conditions for D01 were the analyses incorporating standard surface and upper-level observations and the NCEP global $1^\circ \times 1^\circ$ fields as the analysis background.

Three D02-domain assimilation and simulation experiments (Table 1), designated as CNTL, DA-QR and

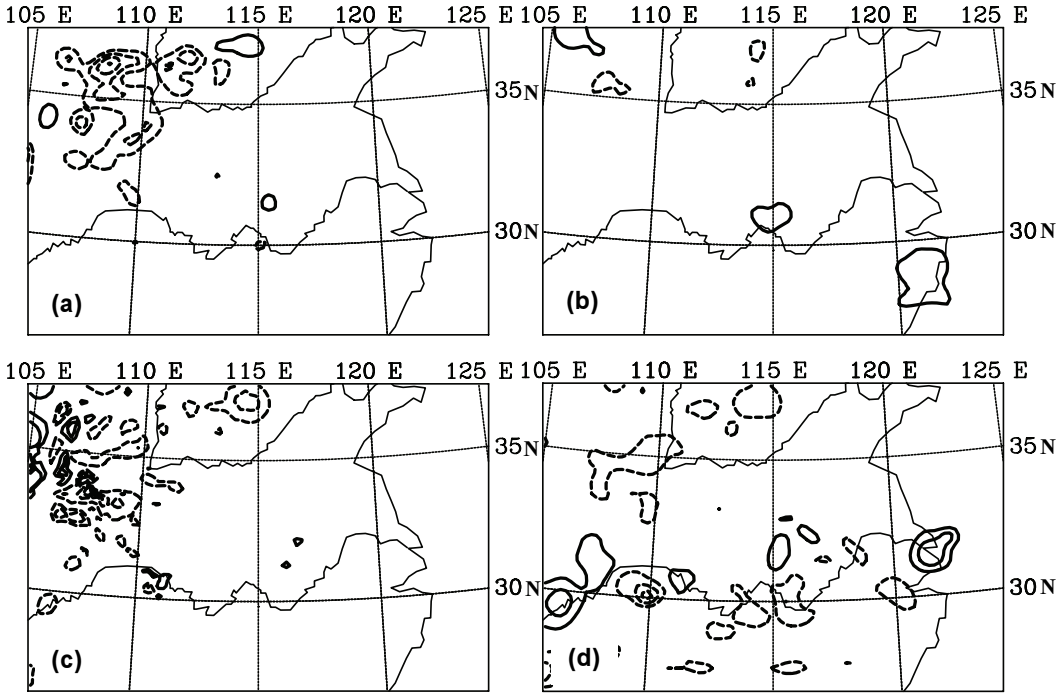

Fig. 6. Same as Fig. 5, except presenting the differences between DA-Q and CNTL.

Table 1. List of numerical experiments.

Experiment	Data assimilated	Variable updated by data assimilation
CNTL	None	None
DA-QR	U, V, T, Q, 6-h Rainfall	All
DA-Q	U, V, T, Q	All
Sens-U	U, V, T, Q, 6-h Rainfall	Only U updated
Sens-V	U, V, T, Q, 6-h Rainfall	Only V updated
Sens-T	U, V, T, Q, 6-h Rainfall	Only T updated
Sens-Q	U, V, T, Q, 6-h Rainfall	Only Q updated

DA-Q, were conducted to assess the impact of observed rainfall assimilation on the simulation of the MCSs along the mei-yu front and the corresponding precipitation during the assimilation window (here after P1) and the ensuing 12-hour forecast period (hereafter P2 and P3). In CNTL, the NCEP global analysis combined with the standard surface and upper-level observations were used as the initial and lateral conditions. In the DA-QR, 4DVAR assimilation of the horizontal winds, temperature, moisture observations and the 6-h accumulated rainfall observations was performed from 1200 UTC to 1800 UTC, whereas experiment DA-Q was the same as DA-QR except for the rainfall data that are excluded from the assimilation.

To further assess the relative impact of the different components of the analysis increment fields on the simulation of this heavy rainfall event, a set of additional, sensitive experiments (Sens-U, Sens-V, Sens-Q and Sens-T, see Table 1) were conducted by adding the analysis increment fields at the initial time, that were obtained from DA-QR, to the analysis background, one at a time. These experiments examined specifically the adjustment to the analysis background on the subsequent simulation. All experiments are listed in Table 1.

4. Numerical results

4.1 *The performance of the minimization*

To evaluate the performance of the 4DVAR experiments, the convergence of the minimization process is first examined. In experiments DA-QR and DA-Q, the minimization was stopped at 93 and 51 iterations, respectively. Figure 4 shows the variations of the cost functions with respect to the iterations; the solid line represents DA-QR, while the dashed line represents DA-Q. As displayed in Fig. 4, the cost functions de-

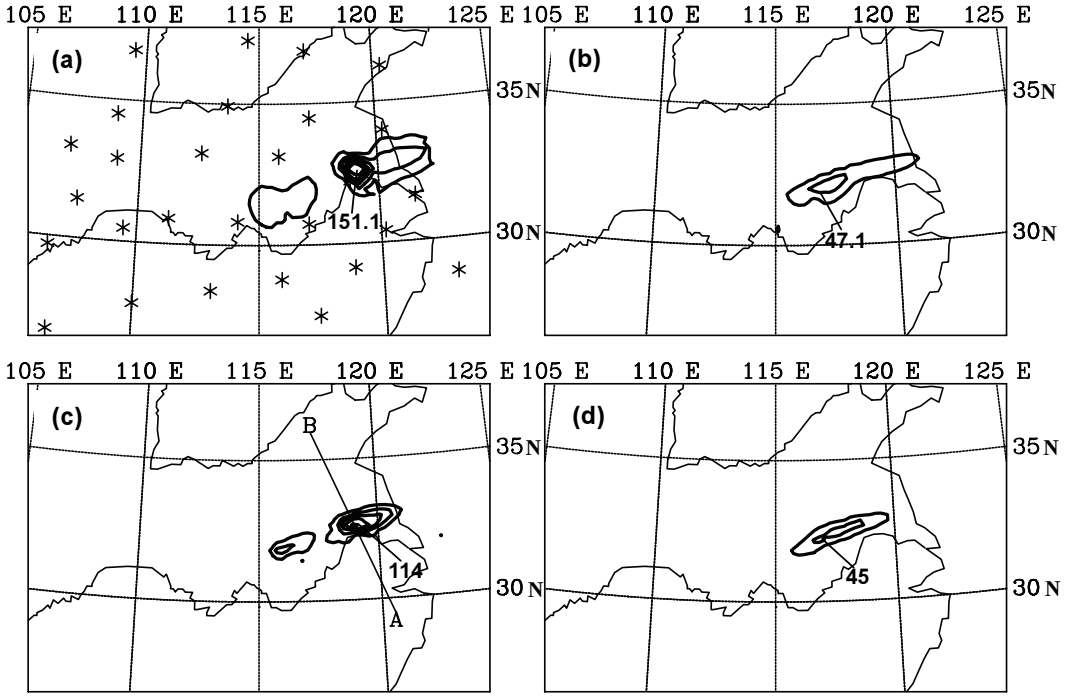

Fig. 7. The 6-h accumulated rainfall valid at 1800 UTC 4 July 2003. (a) observations, (b) CNTL, (c) DA-QR, and (d) DA-Q. The contours start at 10 mm with intervals of 25 mm. The stars in (a) represent the conventional sounding locations used in this study.

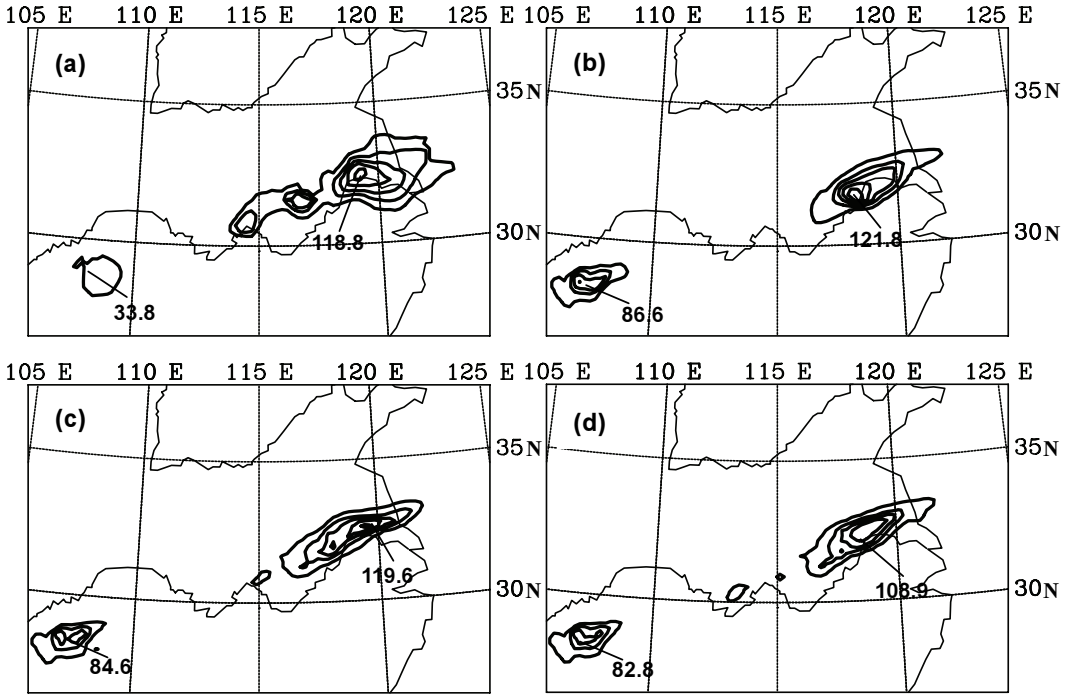

Fig. 8. Same as Fig. 7, but for the 6-hour forecast period ending at 0000 UTC 5 July 2003.

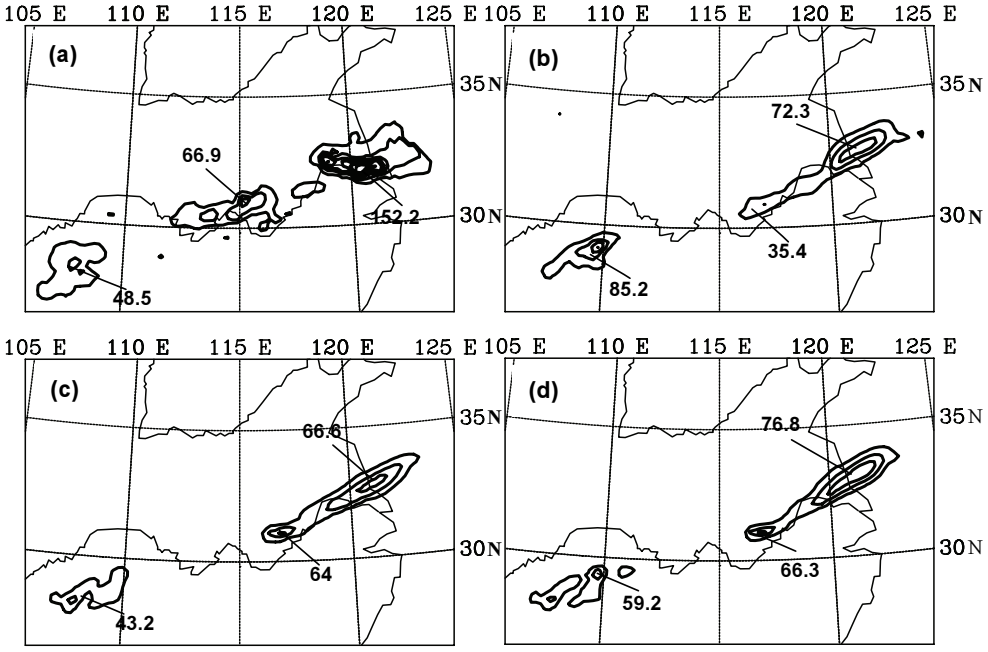

Fig. 9. Same as Fig. 7, but for the 6-hour forecast period ending at 0600 UTC 5 July 2003.

scend significantly in DA-QR and DA-Q, and most of the decrease is achieved within the first 30 iterations. The gradients of the cost function also decrease significantly, with about two orders of magnitude reduction (not shown). Therefore, the minimization in these assimilation experiments was achieved, in spite of the presence of nonlinear physics.

Figure 5 shows the differences in the horizontal winds, temperature and specific humidity fields at 850 hPa level, between DA-QR and CNTL at 1200 UTC July 4. It can be seen that the differences along the Yangtze River at this level are mostly confined to small areas located to the lees of the Dabie and Huangshan Mountains (c.f., Fig. 3), and located upwind of the observed MCSs and rainfall center (c.f., Fig. 2). It should be noted that the features in the difference fields for the different variables have different horizontal scales—those in the horizontal winds and moisture difference fields have scales of about 300–500 km, while the temperature difference field contains small structures of about 50 km in size. Evidently, these difference structures represent mesoscale or sub-synoptic structures that cannot be captured by the standard synoptic observation network, but are created through 4DVAR assimilation of additional observations. By comparing the fields at different levels, we see that most of the differences are found at the low levels (not shown).

The corresponding difference fields between DA-Q and CNTL are shown in Fig. 6. Compared with Fig. 5, it is evident that without rainfall data, the adjustment to the initial background by the assimilation is much smaller, in both magnitude and spatial scale. The impact of assimilating the 6-hour accumulated rainfall data on the assimilated fields is significantly larger than the assimilation of the conventional observations.

4.2 *The impact of rainfall assimilation on simulation*

As shown in Fig. 5, more mesoscale features are included in the estimated state of atmosphere at the initial time after the 4DVAR assimilation of rainfall observations, which will be shown to improve the triggering of convection and the initialization of the MCSs. Consequently, the simulation of the structure and evolution of perturbations at difference scales within the mei-yu front could be improved. The improvement to the simulation of this heavy rainfall event by the 4DVAR assimilation is examined in more details in the following, with an emphasis on several aspects that are closely related to the heavy rainfall during the assimilation window (P1) and the ensuing 12 hour period of simulation (P2 and P3).

4.2.1 *The improvement of the precipitation simulation*

Figure 7 shows the model-simulated, 6-h accumulated rainfall from experiments CNTL, DA-QR, and DA-Q during the assimilation window (P1), as compared to the observations during this same period. Fig. 7a shows that the primary observed heavy rainfall cen-

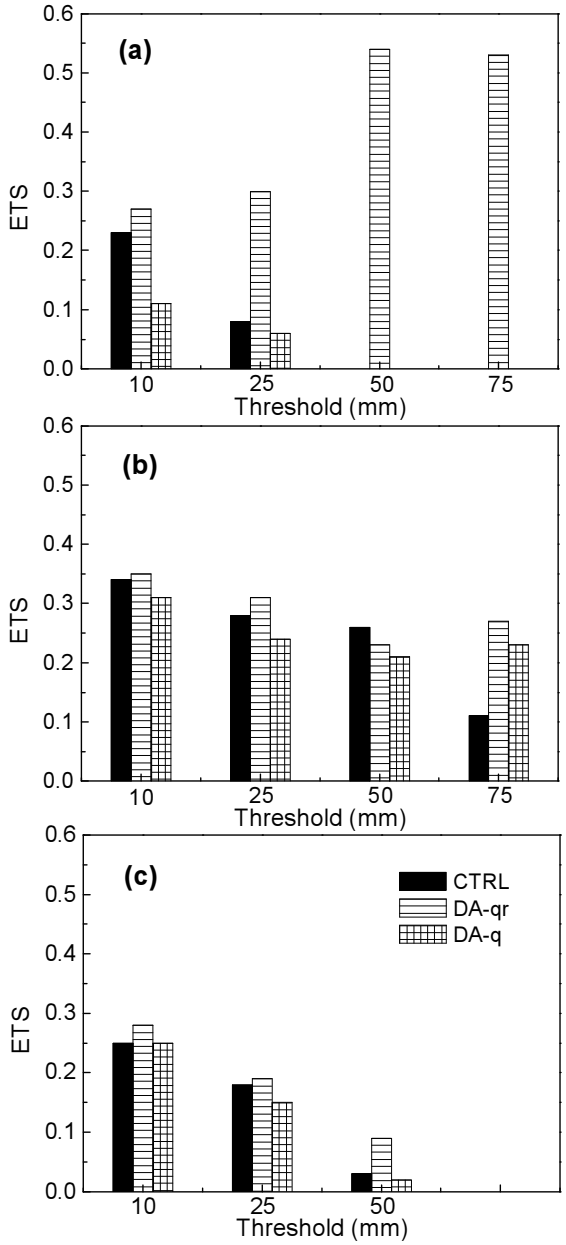

Fig. 10. The equitable threat scores, calculated for the 6-h accumulated rainfall simulations in CNTL, DA-QR, and DA-Q, for different threshold values in (a) P1, (b) P2, (c) P3.

ter is located at Chuzhou (c.f., Fig. 3), with a maximum of about 150 mm. Another much weaker rainfall center, of about 10 mm, is located about 300 km upstream. These precipitation centers are well reproduced by DA-QR (Fig. 7c), in which rainfall data are assimilated. The maximum rainfall amount was measured to be 114 mm in DA-QR, versus the observed 150 mm. Compared to DA-QR, CNTL and DA-Q did a poor job in reproducing the observed rainfall amount and pattern (Figs. 7b and 7d). In both cases, a single center, located off to the west of the true maximum, is obtained; the maximum rainfall in these simulations was slightly above 35 mm. The rainfall pattern in DA-Q was not improved over that of CNTL, except that the maximum center is closer to the position observed (Fig. 7d). It is clear that the 4DVAR assimilation of rainfall data correctly improves the correlation between rainfall simulated by the model and the observations.

The corresponding rainfall fields in the subsequent 6 hour simulation are shown in Fig. 8, together with the observed rainfall. In these observations, we can see that there are four observed heavy rainfall centers along the Yangtze River, located in Guizhou, Hubei, Anhui and Jiangsu provinces, with the maxima of about 30, 40, 70 and 120 mm (Fig. 8a), respectively. In the CNTL, there are only two simulated rainfall centers located in Guizhou and eastern Anhui, and the primary center is located about 100 km southwest of the observed one (Fig. 8b). However, the maximum of 120 mm is close to what the observed value of 118 mm. The two experiments that include data assimilation, i.e., DA-QR and DA-Q, were more successful in capturing the observed precipitation pattern. Specifically, at least one of the two weak centers in the middle is captured in these two experiments, though at somewhat weaker intensities than in the observation. The rainfall center near Wuhan, Hubei province is better simulated in the DA-QR at almost the exact location as in observations. The location and intensity of the primary precipitation center located in Jiangsu are also better captured, with a maximum value of 119.6 mm in DA-QR that is very close to the obtained 118.8 mm. There is an indication of a secondary maximum in the main area of precipitation (Fig. 8c) that may be linked to the second maximum center from the east that is found in the observations (Fig. 8a).

During the next 6-hour period of simulation, between 0000 and 0600 UTC July 5, the results of all three experiments converged toward one another (Fig. 9), with a general tendency for the primary rain band to move out into the sea faster than was observed, although the error was still lowest in DA-QR (Fig. 9c). The primary rainfall center in Jiangsu was too weak in all three experiments, but the rainfall maximum in Hubei was correctly simulated in both DA-QR and DA-Q (Fig. 9c, d) but was too weak in CNTL. The center in the southwestern Guizhou province was reasonably captured by all three experiments.

To more quantitatively measure the effectiveness of the rainfall assimilation, the equitable threat scores (hereafter ETS; e.g., Schaefer, 1990) were calculated. The main merit of the ETS, when compared to the

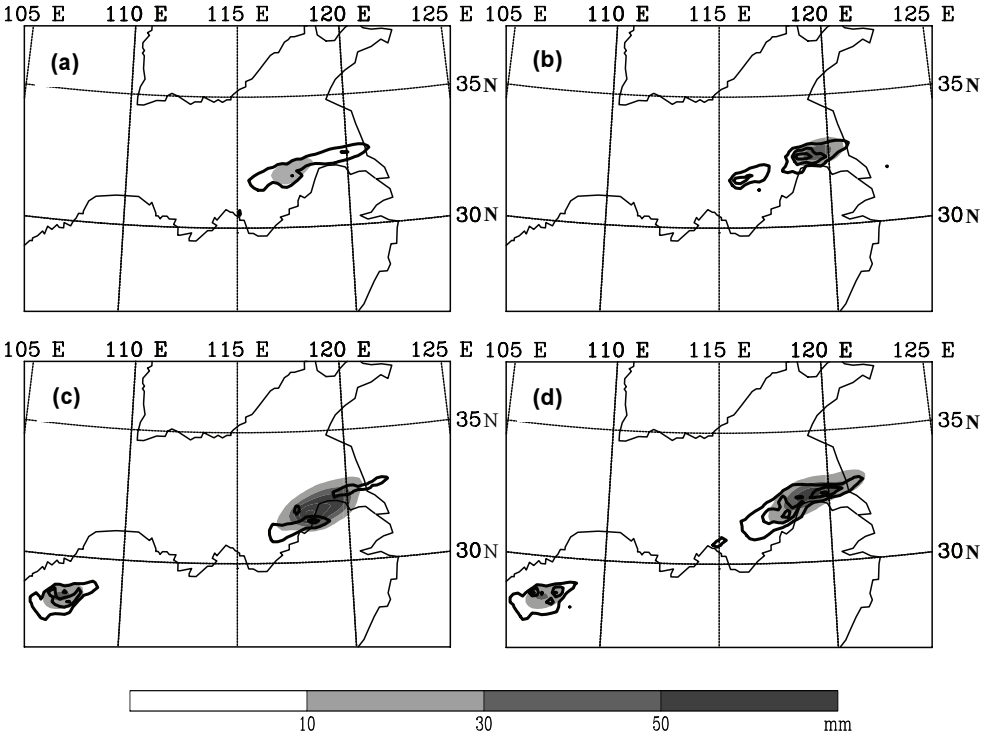

Fig. 11. The simulated, 6-h explicit (shaded) and implicit rainfall (solid, greater than 10 mm, contour interval is 25 mm) during the assimilation window for (a) CNTL and (b) DA-QR; and in P2 for (c) CNTL, and (d) DA-QR.

original threat score, is the allowance for the scores to be compared more fairly across different regimes by excluding the hits associated with random chance, so it is often used in the verification of rainfall forecasting in NWP models. In this study, the rainfall observations were interpolated onto the model grid using the Cressman method; thus all ETSs were calculated in the model domain.

The significant improvement in ETS by rainfall assimilation is clearly evident during the assimilation period. Figure 10a, shows that the best agreement between the model and observed rainfalls was obtained via DA-QR for all threshold values. It is remarkable that the ETSs of DA-QR and their differences from the scores of the other two experiments actually increase with the threshold values; particularly, the ETSs of DA-QR for precipitation thresholds of 50 and 75 mm were close to 0.6, while the scores of DA-Q and CNTL were zero, thereby confirming our earlier qualitative assessment of the precipitation simulations in DA-QR during this period. However, the ETSs of DA-Q during this period were no better than those of CNTL.

The improvement resulting from the rainfall assimilation remains in P2 (Fig. 10b) as the ETSs in DA-QR were still the largest for all but the 50 mm thresholds. However, the differences among the ETSs of the three experiments were not large, except for the largest threshold of 75 mm, for which DA-QR improves the score by more than a factor of two. During the next 6 hours of simulation, the ETSs are generally lower, but DA-QR continues to have the best scores, especially for the larger threshold (Fig. 10c).

From the analysis, it can be found that the rainfall assimilation is most crucial in the convection triggering stage (P1), while when the convections are fully initialized in P2 and P3, the positive effects of rainfall assimilation are still moderate but not as remarkable as in P1.

To see how the rainfall data assimilation impacted the grid-scale explicit precipitation and the implicit parameterized precipitation, we plotted the explicit and implicit rainfall in Fig. 11, for the two 6 hour periods from CNTL and DA-QR. It can be seen that, after rainfall assimilation, the intensity of explicit precipitation was greatly enhanced and the location was moved into the downstream region, while the implicit precipitation had almost the same pattern and its intensity was enhanced (Figs. 11a, b). Similar results are shown in P2, except that the rainfall center located in Anhui was captured mainly through the modification of the implicit precipitation (Figs. 11c, d). As for this mei-yu heavy rainfall simulation, both the explicit

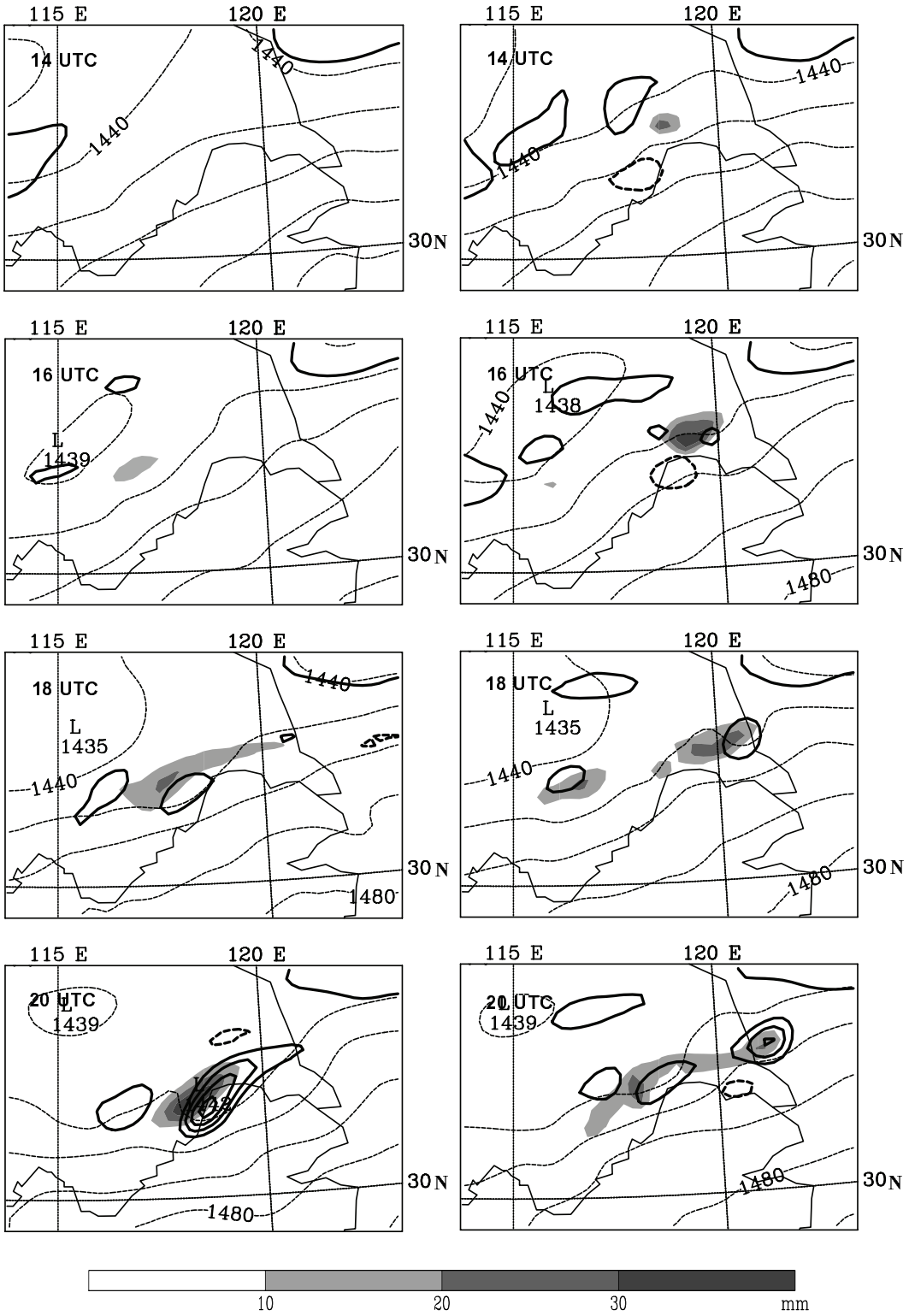

Fig. 12. The hourly accumulated rainfall (shaded, greater than 10 mm, contour interval is 10 mm), relative vorticity (thick, negative dashed; contour interval is 8×10^{-5} s^{-1}) and geopotential height (thin, dotted; contour interval is 10 m) on 850 hPa valid from 1400 UTC July 4 to 0000 UTC July 5. Left panel: CNTL; right panel: DA-QR.

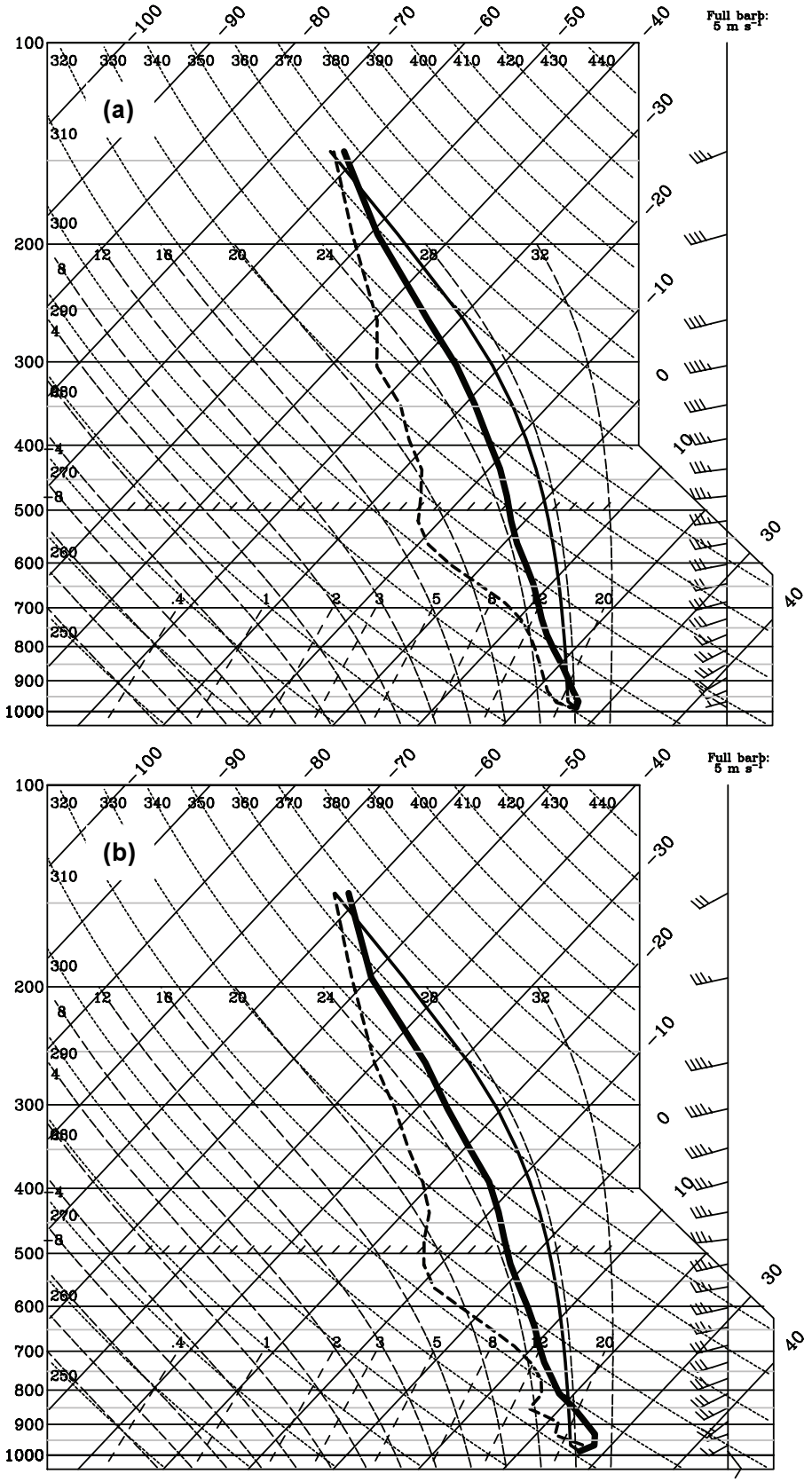

Fig. 13. Model sounding (skew-T) at Chuzhou in Fig. 3 for (a) CNTL and (b) DA-QR at 1200 UTC July 4.

and implicit precipitation had comparable importance; however, in the mountainous area, the cumulus parameterized process was much more critical, due to the complicated terrain. Presumably, after rainfall assimilation, the modifications in lower-level moisture were favorable to the genesis of the explicit rainfall, while the modifications in the horizontal wind fields might have strengthened the lower-level convergence, which is favorable to the triggering of the cumulus parameterization. Actually, in one set of experiments, the moisture and meridional wind were found to be much more critical in rainfall simulation than the other initial fields, which may support our above hypothesis.

4.2.2 *MCSs simulation and precipitation spin-up*

Many MCSs or low-level vortices often develop along the mei-yu front during the warm season in Eastern China. These MCSs that are embedded in the mei-yu front are the main cause of the heavy rainfall within the frontal region and are tightly connected with the mesoscale vortices (Chen et al., 1998, 2000). Therefore, to simulate the heavy rainfall processes correctly, it is essential to correctly simulate the initiation, location, spatial distribution and evolution of the MCSs.

Figure 12 shows the geopotential height and relative vorticity at the 850 hPa level, together with hourly accumulated rainfall. Similar to Chen et al. (1998), we use the rainstorms to represent the MCS here. From Fig. 12, it can be seen that several separated mesoscale cyclonic vortex centers quickly formed during the first few hours in DA-QR, in the DRYR, whereas there were no similar perturbation structures in CNTL. At 1400 UTC July 4, a rainstorm center accompanied by a mesoscale, cyclonic, vortex center was seen in DA-QR, which means that the precipitation had been spun-up. At 1600 UTC, the rainstorm center increased in size and two hours later, several rainstorm centers appeared, that were accompanied by a train of vortex centers. In CNTL, the first sign of heavy precipitation does not appear until 1600 UTC and the areas remain smaller. From 2200 UTC on, the separate vortex centers began to merge and move eastward, and the heavy rain area shrinks slightly (not shown and c.f., Fig. 2). Compared with the brightness temperature in Fig. 2, the initiation, location, evolution and spatial distribution of MCSs are better captured via DA-QR. However, the geopotential height field was impacted very little by the data assimilation in DA-QR.

In CNTL, the genesis, maturing and movement of the MCSs were also simulated. However, the MCSs initiation in CNTL occurred about 2 to 4 hours later than in DA-QR, indicating a longer spin-up time than the DA-QR model took for precipitation. Furthermore, CNTL does not exactly simulate the location and the spatial distribution of the MCSs and there were no separate vortex centers.

To see the impact of assimilating rainfall observations on the local conditions within the heavy rain area, we examine the extracted model soundings at 1200 UTC at Chuzhou (c.f., Fig. 3) where the primary observed heavy rainfall center was located (Fig. 13). In comparison with Fig. 13a and b, the surface temperature was increased by a modest 1°C in DA-QR and the convective available energy (CAPE) was increased from 433 J kg^{-1} in CNTL to 2220 J kg^{-1} via the data assimilation. Therefore, a more favorable local condition for convection was created by the data assimilation, including rainfall data. Such adjustments to the initial conditions and CAPE features were similar to the those made and reported in other rainfall assimilation studies (e.g., Zou and Kuo, 1996; Peng and Zou, 2002).

From the above analyses, it can be concluded that after rainfall assimilation, the local condition at the initial time was modified to be more favorable for the convection triggering and consequently the spin-up time required for precipitation was greatly reduced. Based on these adjustments, the forecast of the triggering, location and evolution of MCS along the mei-yu front was also improved after the assimilation period.

4.2.3 *The modifications to the low-level jet (LLJ)*

In the mei-yu front, the embedded MCSs have significant correlations with the low level jet (LLJ). The LLJ plays a positive role in feeding the convection, by transporting warm and moist air from south China towards the mei-yu front, providing a low-level convergence downstream of the jet core and helping to establish a favorable, convectively unstable environment (Chen et al., 2005, and references in their introduction). Therefore, a successful simulation of the LLJ is also important for the correct initialization and evolution of MCSs and for forecasting the heavy rainfall associated with the mei-yu front.

Figure 14 presents the horizontal wind and speed fields at the 850 hPa level, and the 3-h accumulated rainfall. With data assimilation, a mesoscale, low-level jet (mLLJ), defined as regions with horizontal wind speeds exceeding 16 m s^{-1}, is present at 1200 UTC, with two local wind speed maxima located over Hubei and Anhui. At 1500 UTC, the mLLJ located in Anhui was further enhanced in the DA-QR and a heavy rainfall center appeared at the nose of the mLLJ, but no distinct mLLJ center or rainfall center was present in the CNTL at this time. Three hours later, in DA-QR, the mLLJ in Hubei was enhanced as well, in front of which, another heavy rainfall center appears. Up until this time, no regions with wind speeds exceeding

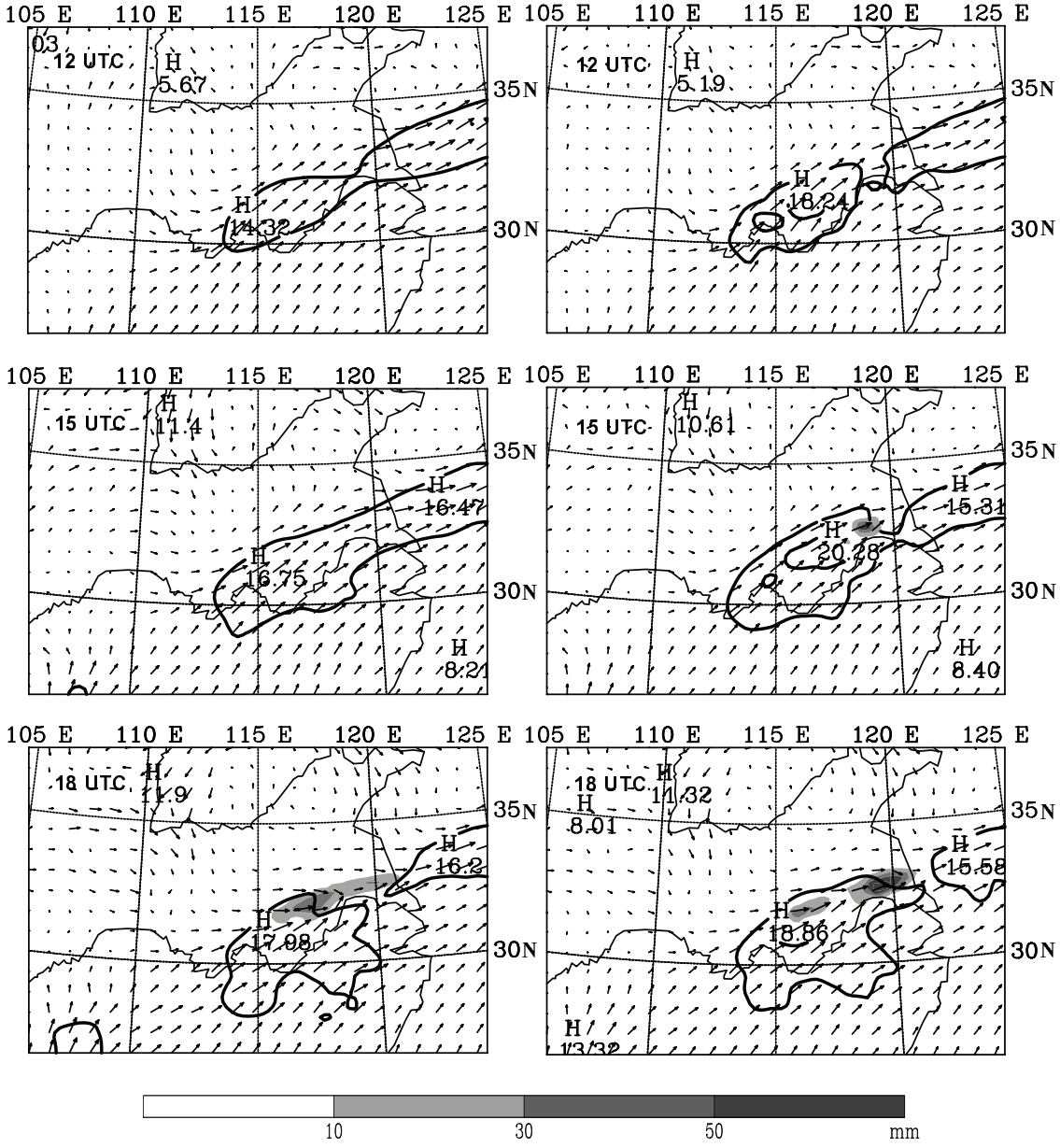

Fig. 14. The horizontal wind speed (greater than 12 m s^{-1}, solid; contour interval is 4 m s^{-1}), horizontal wind (arrow) on 850 hPa valid at 1200, 1500, and 1800 UTC July 4 and 3-h simulated accumulated rainfall (shaded; contour interval is 10 mm) valid at 1500 and 1800 UTC July 4. Left panel: CNTL; right panel: DA-QR.

16 m s^{-1} were present in CNTL. In DA-QR, the simulated regions of high wind speed extended further to the northeast than in CNTL and were stronger, which might explain why the heavy rainfall center in DA-QR lay further northeastward during the assimilation period (Fig. 14). Similar features were found during the subsequent simulations (not shown).

From Fig. 14, one can see that the heavy rainfall centers were always located ahead of the mLLJ, which suggests interactions exist between the MCSs and the mLLJ. In DA-QR, the local condition within the DRYR was modified to be favorable for the initiation of the MCSs. On the other hand, the evolution of the MCSs would induce and strengthen the mLLJ, and its enhancement would in turn increase the supply of moisture and thereby create a stronger, low-level convergence at its nose region for the development and maintenance of the MCSs. Therefore, the improved simulation of mLLJ, LLJ and MCSs by the rainfall assimilation leads to a more successful simulation of

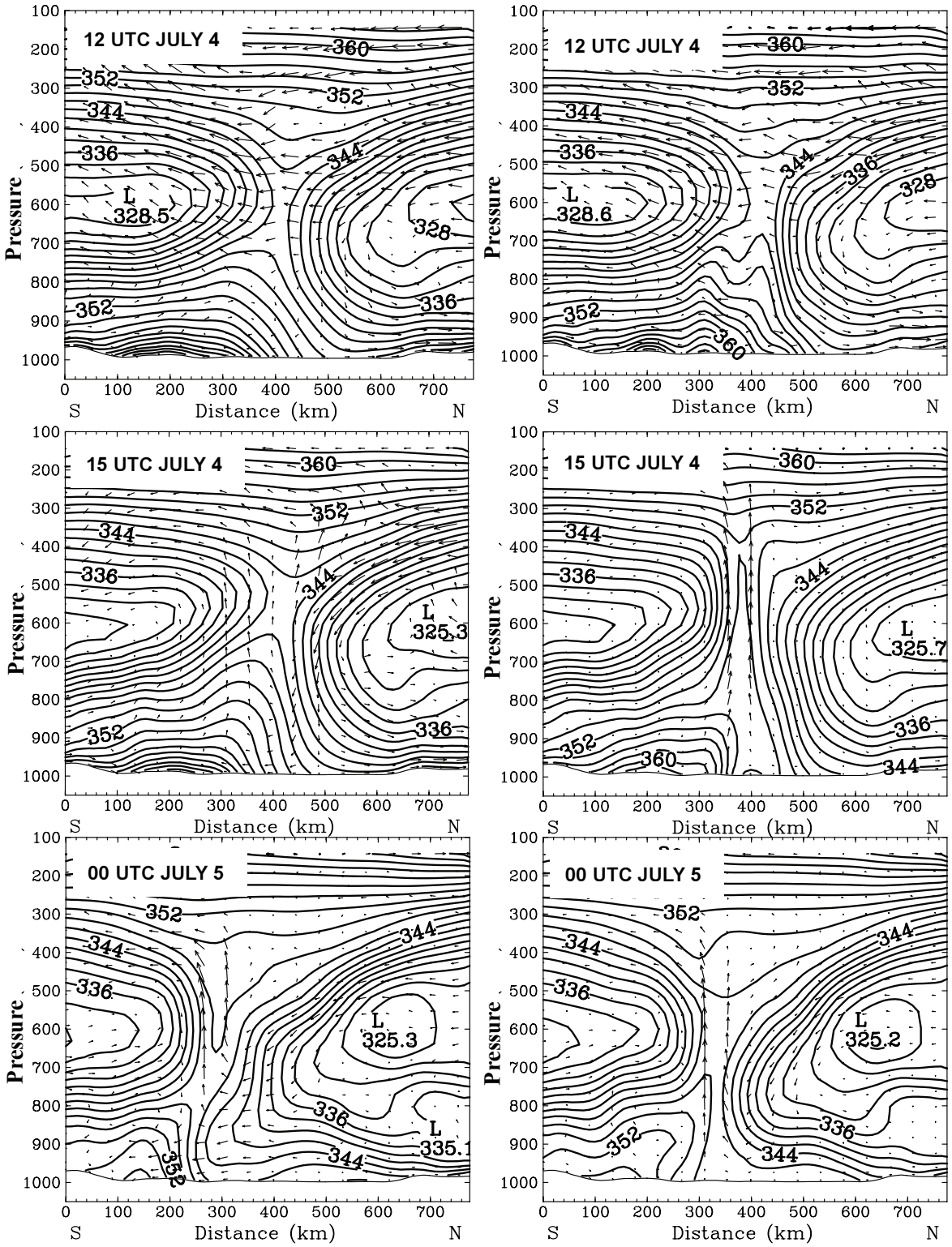

Fig. 15. Mean cross-section, along line AB in Fig. 7c, of equivalent potential temperature (solid; contour interval is 2 K) and winds (arrows), the average distance into and out of the cross-section is 80 km. Left panel: CNTL; right panel: DA-QR.

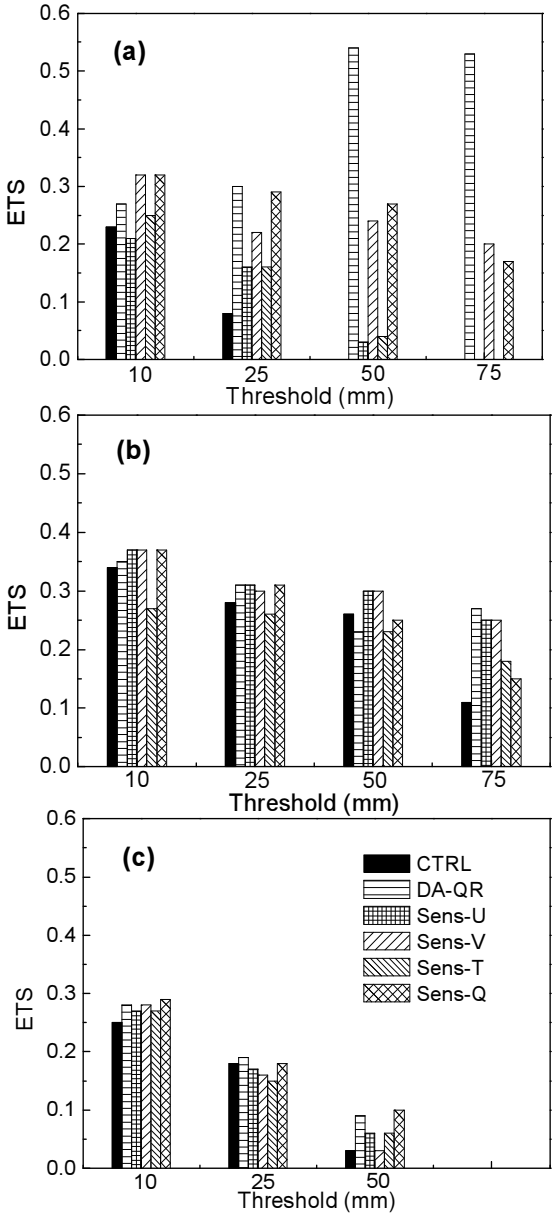

Fig. 16. Same as Fig. 10, except for the experiments CNTL, DA-QR, Sens-U, Sens-V, Sens-T and Sens-Q.

the heavy rainfall processes as a whole. We note here that the rainfall assimilation had little impact on upper-level jet streak (not shown).

4.2.4 *Synoptic and sub-synoptic structures of the mei-yu front*

In addition to the improvements in the simulation of the mesoscale systems, including the MCS and the mLLJ by the data assimilation, the sub-synoptic structure of mei-yu front is also modified both during the assimilation window and during the subsequent simulation. Figure 15 shows the cross sections along line AB in Fig. 7c for mean equivalent potential temperature and winds in CNTL and DA-QR, at 1200 and 1500 UTC July 4. The averaging region extends from line AB for 40 km in the both eastward and westward directions, and the cross section goes right through the primary observed heavy rainfall center during this period (c.f., Fig. 7c). It can be seen that the data assimilation in DA-QR also had a moderate impact on the sub-synoptic structure of the mei-yu front initially. With rainfall assimilation, there were flunctuations in the equivalent potential temperature within the middle and lower levels over the heavy rainfall region. In the middle and lower levels, the gradient of the equivalent potential temperature was increased, its contours were steeper and the frontal circulation was slightly enhanced. Three hours later, at 15 UTC July 4, the changes to the simulated mei-yu front were even more clear: the front was stronger and steeper and the convection was much stronger. At 0000 UTC July 5, an even larger difference between the structures of simulated mei-yu front in DA-QR and CNTL were found. In the CNTL there was significant cross-frontal winds only in the low-level and the front was pushed southward, while in DA-QR, there was a strong vertical motion from the lower to mid-high levels and there the front appeared strong as well. From the above analysis, it can be seen that, the small, convective scale perturbations introduced by the assimilation of rainfall could favor the triggering of the MCSs and through the interactions between the MCSs and the other mei-yu weather systems, the influences were then propagated upscale to the meso- and sub-synoptic scales. Thus, in this case, the 4DVAR of rainfall assimilation was able to improve the simulation of multi-scale weather systems that are associated with the mei-yu heavy rainfall.

5. Sensitivity experiments

Thermodynamic fields, including temperature and moisture, are generally considered crucial for convection triggering and precipitation forecasting. To better understand the impact of adjustments to different variables by the data assimilation for the current mei-yu front heavy rainfall event, a set of additional experiments were carried out to assess the relative impact of the different components of the analysis increments that were produced by the data assimilation on the precipitation simulation. Similar to Peng and Zou (2002), we substituted the zonal wind, meridional wind, temperature and moisture fields into CNTL, one by one, with the corresponding adjusted field from DA-QR at the initial time, and used these partly updated states to initialize the experiments Sens-U, Sens-V,

Sens-T and Sens-Q, respectively (Table 1).

The ETSs of these experiments are presented in Fig. 16. During the first 6-hour period where the ETSs are shown, the convection was being initiated, while in the second period, the MCSs became mature. During the first 6-hour period, or within the assimilation window, the ETSs of all the sensitivity experiments were higher than that of the CNTL, while remaining lower than that of DA-QR (Fig. 16a). Furthermore, the ETSs of Sens-V and Sens-Q were higher than those of the other two sensitivity experiments at all precipitation thresholds, suggesting that the moisture and meridional wind fields are most crucial at this initiation stage of the mei-yu front convection. The meridional winds were associated with the LLJ and mLLJ and represented most of the cross-frontal flows as well. The enhancement to the mLLJ and LLJ, strengthens the low-level convergence, while the enhancement to the moisture field created a more favorable condition for convection and precipitation. The lesser role played by the temperature adjustment was consistent with the fact that the mei-yu fronts were associated with weak temperature gradients or baroclinity, but with strong moisture gradients. In contrast, Peng and Zou (2002) found that the adjustments to temperature and moisture were more important than wind fields for a squall line weather system. Our results indicate a unique aspect of the mei-yu fronts in comparison to most other convective systems.

During the next period, P2, when the MCSs were fully developed, the ETSs for the four sensitivity experiments had only insignicant differences, with the ETSs of Sens-U and Sens-V being slightly higher (Fig. 16b). These indicate that the responses of the precipitation forecasts to the initial conditions were not completely linear. However, at the end of the 12-h integration, many interactions had occurred among the model variables and it was no longer possible to separate the impacts of the individual analysis increments. Because these are the numerical simulations within a limited area, the lateral boundary conditions could also significantly effect the numerical results during the long-term model run, which might have lead the results to converge. One thing worth noting is that for the highest precipitation thresholds (50 and 75 mm), all experiments that included complete or partial analysis increments had better or similar scores than CNTL, during both P2 and P3 periods. For the other thresholds, the relative differences were much smaller.

6. Summary and discussions

In this study, the MM5 4DVAR and prediction system were employed to assimilate rainfall data and other conventional observations for improving the simulation of a particular mei-yu front heavy rainfall event in the downstream regions of the Yangtze River in China. In spite of the use of only conventional 6-h accumulated rainfall observations and the relative coarse grid-mesh used (20-km horizontal resolution for the inner domain), the simulation of this heavy rainfall event was successful, and with the assimilation of rainfall data, positive impacts on the weather systems, ranging from mesoscale to sub-synoptic scales in the mei-yu frontal systems, were found both during the assimilation window and during the 12 hours beyond. By using the partly adjusted initial conditions from the rainfall assimilation, the specific impact of the different analysis increment fields on the simulation of this heavy rainfall event was assessed. More specific results are summarized as follows:

(1) The MM5 4DVAR system, used with relatively simple, though still complete physics, was capable of effectively assimilating large amounts of rainfall observations as well as more conventional data. With the assimilation of the rainfall observations, the simulation of the precipitation intensity and pattern of this heavy rainfall event in East China was greatly improved during the assimilation window and the improvements also extended out to 12 hours beyond the assimilation window. Furthermore, the rainfall assimilation was shown to effectively reduce the spin-up time of precipitation as well.

(2) The overall improvement of the rainfall simulation was mainly achieved through the model's explicit precipitation, while the cumulus parameterized process also played an important role in the rainfall simulation within the mountainous areas.

(3) Rainfall assimilation was able to capture mesoscale features not present in the original NCEP analysis. The main modifications to the state at the initial time by the 4DVAR assimilation were mainly concentrated in the sensitive regions in the lees of the mesoscale mountains, but upwind of the observed MCSs and heavy rainfall centers. The assimilation enhanced mesoscale features, including the mLLJ and MCSs, as well as the mei-yu front circulations, in ways that favored more intense convection.

(4) The adjustments to the moisture and meridional winds by the data assimilation were found to be more important than those made to either the temperature or zonal winds, especially in terms of the precipitation simulation within the assimilation window. This is consistent with the weakly baroclinic nature of mei-yu fronts and the importance of low-level, cross-frontal convergence for their precipitation.

We note here that the improvements to the QPF during the periods beyond assimilation window were

relatively small, even though the model-produced precipitation was much closer to the observed values during the assimilation window and physically consistent mesoscale features were still obtained through the assimilation. Such less-than-satisfactory results required further investigation. The possible presence of model errors in the assimilation system may play a role, while the length of assimilation window for such a nonlinear precipitation system also needs investigation. Unfortunately, the availability of only 6-hour accumulated precipitation data precludes experiments with shorter assimilation windows. Attempts will be made in the future to use higher-frequency data and/or remotely sensed observations when they are available. Despite the existence of previous work assimilating rainfall data using a similar methodology, our work represents this method as applied to a mei-yu great heavy rainfall case over China. Continued research along this line is certainly needed. Initial condition sensitivity studies can also be carried out using the adjoint tools to extend the knowledge base on the predictability of a mesoscale convective storm in mei-yu front.

Acknowledgements. This research was supported by the National Natural Science Foundation of China under Grant Nos. 40325014, 40333031, SRFDP, TRAPOYT, FANEDD 11999, and under the support of The Key Scientific and Technological Project of the Ministry of Education and The State Key Basic Research Program (Grant No. 2004CB18300). The authors are grateful to Dr. J. P. Tang, Dr. L. Zhang and Dr. B. J. Chen for their assistance with the numerical modelling and simulation. The authors also thank the two anonymous reviewers for their precious comments.

REFERENCES

Blackadar, A. K., 1976: Modeling the nocturnal boundary layer. Preprints, Third Symp. on Atmospheric Turbulence, Diffusion, and Air Quality, Raleigh, Amer. Meteor. Soc., 46–49.

Blackadar, A. K., 1979: High resolution models of the planetary boundary layer. *Advances in Environmental Science and Engineering*, Vol. 1, No. 1, J. Pfafflin and E. Ziegler, Eds., Gordon and Breach, 50–85.

Chen, S. J., Y. H. Kuo, W. Wang, Z. Y. Tao, and B. Cui, 1998: A modeling case study of heavy rainstorms along the mei-yu Front. *Mon. Wea. Rev.*, **126**, 2330–2351.

Chen, S. J., W. Wang, K. H. Lau, Q. H. Zhang, and Y. S. Chung, 2000: Mesoscale convective systems along the mei-yu front in a numerical model. *Meteor. Atmos. Phys.*, **75**, 149-160.

Chen, G. T-J., C-C. Wang, and D. T-W. Lin, 2005: Characteristics of low-level jets over Northern Taiwan in mei-yu season and their relationship to heavy rain events. *Mon. Wea. Rev.*, **133**, 20–43.

Dudhia, J., 1993: A nonhydrostatic version of the Penn State-NCAR mesoscale model: Validation tests and simulation of an Atlantic cyclone and cold front. *Mon. Wea. Rev.*, **121**, 1493–1513.

Donner, L J., 1988: An initialization for cumulus convection in numerical weather prediction models. *Mon. Wea. Rev.*, **116**, 377–385.

Fiorino, M., and T. T. Warner, 1981: Incorporating surface winds and rainfall rates into the initialization of a mesoscale hurricane model. *Mon. Wea. Rev.*, **109**, 1914–1929.

Grell, G. A., J. Dudhia, and D. R. Stauffer, 1995: A description of the fifth-generation Penn State/NCAR Mesoscale model (MM5). NCAR Tech. Note, NCAR/TN-398 t STR, 138pp. [Available from NCAR Publications Office, P. O. Box 3000, Boulder, CO 80307–3000]

Guo, Y. R., Y. H. Kuo, J. Dudhia, and D. Parsons, 2000: Four-dimensional variational data assimilation of heterogeneous mesoscale observation for a strong convective case. *Mon. Wea. Rev.*, **128**, 619–643.

Kato, T., and Coauthors, 2003: Reason for the failure of the simulation of heavy rainfall during X-BAIU-01—importance of a vertical profile of water vapor for numerical simulation. *J. Meteor. Soc. Japan*, **81**, 993–1013.

Krishnamurti, T. N., J. Xue, H. S. Beti, K. Ingles, and D. Oosterhof, 1991: Physical initialization for numerical weather prediction over tropics. *Tellus*, **43AB**, 53–81.

Krishnamurti, T. N., H. S. Beti, and K. Ingles, 1993: Physical initialization using SSM/I rain rates. *Tellus*, **45A**, 247–269.

Liao Jie, and Tan Zhemin, 2005: Numerical simulation of a heavy rainfall event along the mei-yu front: Influences of different scale weather systems. *Acta Meteorologica Sinica*, **63**, 771–788. (in Chinese)

Park, S. K., and D. Zupanski, 2003: Four-dimensional variational data assimilation for mesoscale and storm-scale applications. *Meteor. Atmos. Phys.*, **82**, 173–208.

Peng, S. Q., and X. Zou, 2002: Assimilation of NCEP multi-sensor hourly rainfall data using 4D-Var approach: A case study of the squall line on April 5, 1999. *Meteor. Atmos. Phys.*, **81**, 237–255.

Pu, Z.-X., and W.-K. Tao, 2004: Mesoscale assimilation of TMI rainfall data with 4DVAR: Sensitivity studies. *J. Meteor. Soc. Japan*, **82**, 1389–1397.

Schaefer, J. T., 1990: The critical success index as an indicator of warning skill. *Wea. Forecasting*, **5**, 570–575.

Tsuyuki, T., 1997: Variational data assimilation in the Tropics using precipitation data. Part III: Assimilation of SSM/I precipitation rates. *Mon. Wea. Rev.*, **125**, 1447–1463.

Wang Yunfeng, Wang Bing, Han Yueqi, Zhu Min, Hou Zhiming, Zhou Yi, Liu Yudi, and Kou Zheng, 2004: Variational Data Assimilation Experiments of mei-yu

Front Rainstorms in China. *Adv. Atmos. Sci.*, **20**(3), 479–486.

Zhang, D.-L., and R. A. Anthes, 1982: A high–resolution model of the planetary boundary layer—Sensitivity tests and comparisons with SESAME-79 data. *J. Appl. Meteor.*, **21**, 1594–1609.

Zou, X., F. Vandenberghe, M. Pondeca, and Y.-H. Kuo. 1997: Introduction to adjoint techniques and the MM5 adjoint modeling system. NCAR Tech. Note TN-435-STR, 177pp. [Available from National Center for Atmospheric Research. P. O. Box 3000, Boulder, CO 80307–3000.]

Zou, X., W. Huang, and Q. Xiao, 1998: A user's guide to the MM5 adjoint modeling system. NCAR TN-437+IA. MMM division, NCAR, 97pp. [Available from National Center for Atmospheric Research, P. O. Box 3000, Boulder, CO 80307–3000.]

Zou, X. L., and Y. H. Kuo, 1996: Rainfall assimilation through an optimal control of initial and boundary conditions in a limited-area mesoscale model. *Mon. Wea. Rev.*, **124**, 2859–2883.

Zupanski, M., and D. Zupanski, 2002: Four-dimensional variational data assimilation for the Blizzard of 2000. *Mon. Wea. Rev.*, **130**, 1967–1989.

Zupanski, D., and F. Mesinger, 1995: Four-dimensional variational data assimilation of precipitation data. *Mon. Wea. Rev.*, **123**, 1112–1127.